Applied Physics Letters ARTICLE pubs.aip.org/aip/apl

Enhanced intensity of Raman signals from hexagonal boron nitride films

Cite as: Appl. Phys. Lett. **123**, 073101 (2023); doi: 10.1063/5.0159365
Submitted: 23 May 2023 · Accepted: 3 August 2023 ·
Published Online: 16 August 2023

View Online Export Citation CrossMark

F. Schaumburg,[a] S. Sleziona, M. Zöllner, V. Dergianlis, M. Schleberger, M. Geller, A. Lorke, and G. Prinz

AFFILIATIONS

Faculty of Physics and CENIDE, University of Duisburg-Essen, Lotharstr. 1, 47057 Duisburg, Germany

[a]Author to whom correspondence should be addressed: felix.schaumburg@uni-due.de

ABSTRACT

Optical spectroscopy is commonly used to study the properties of 2D materials. In order to obtain the best signal-to-noise ratio, it is important to optimize the incoupling of the excitation laser and, at the same time, reduce spurious light reflection. We performed Raman spectroscopy on exfoliated hexagonal boron nitride (hBN) flakes of different thicknesses, placed on a 300 nm SiO_2 on Si substrate. By changing the hBN layer thickness, we found a specific thickness, where the Raman signals from the substrate and the hBN showed maximum intensity, whereas the backscattered laser light was suppressed. To explain the increased emission, we calculated the reflectivity and transmissivity of the full layer system (air, hBN, SiO_2, and Si) as a function of hBN layer thicknesses for different excitation wavelengths (457, 532, and 633 nm), using the transfer-matrix algorithm. To compare theory with the experiment, we performed Raman measurements with these three different excitation wavelengths on different flakes and determined their thicknesses with AFM measurements. The experimental results are in good agreement with the calculations, which shows the importance of thin film interference to obtain optimum spectroscopic conditions. Since interference colors are easily visible in an optical microscope, this facilitates the choice of optimum flakes for a wide range of optical characterization techniques, including Raman, photoluminescence, and single defect spectroscopy.

© 2023 Author(s). All article content, except where otherwise noted, is licensed under a Creative Commons Attribution (CC BY) license (http://creativecommons.org/licenses/by/4.0/). https://doi.org/10.1063/5.0159365

21 August 2023 14:13:57

The interest in van der Waals materials grew very rapidly since the first realization of graphene by Andre Geim and Konstantin Novoselov in 2004.[1] Later, it was found that encapsulation of such materials in hexagonal boron nitride (hBN) leads to a drastic improvement of their electronic and optical properties.[2] The van der Waals material hBN provides materials like graphene or transition metal dichalcogenides (TMDCs) with protection from oxidation.[3,4] On the other hand, hBN itself can host optically active single defects, which are of great interest as room-temperature single photon emitters.[5–13] Therefore, hBN also belongs to the class of 2D materials, which might serve as building blocks for future quantum technologies. For such applications, optical excitation and light extraction efficiency are key parameters.

It was found that hBN-based emitters exhibit very different brightness, depending on the preparation conditions of the flakes.[5–13] To further elucidate these results, we investigate hBN flakes of different thicknesses on a standard Si/SiO_2 substrate. The flake thicknesses, ranging from a few monolayers up to 290 nm, were determined by atomic force microscopy (AFM). The Raman peak intensities were studied as a function of thickness and excitation wavelength, and we found that they oscillate with the hBN thickness. The results were then compared to model calculations using the transfer-matrix algorithm (TMA).[14–17] The measured data are in good agreement with the model. The thickness-dependent difference in reflectivity and transmissivity also explains the colorful appearance of different flakes in a microscope image. Our findings can be used not only to easily approximate hBN layer thicknesses by optical microscopy but also to select hBN flakes with enhanced light emission.[18–20]

Our samples are mechanically exfoliated hBN flakes, placed on top of a Si substrate with a $d_{SiO_2} = 300 \pm 15$ nm thick layer of SiO_2 [see Fig. 1(b)]. Figure 1(a) shows a microscope image of the substrate surface with hBN flakes of different layer thicknesses. Here, we can already see the different colors due to the difference in the layer thickness, caused by the well-known thin film interference effect (see, e.g., Ref. 21). The Raman measurements were performed in backscattering geometry [see Fig. 1(b)], using two different spatially resolved Raman spectrometers. One is a custom-built setup with a 532 nm excitation laser and a 50× objective (NA = 0.85), resulting in a spot size of

© Author(s) 2023

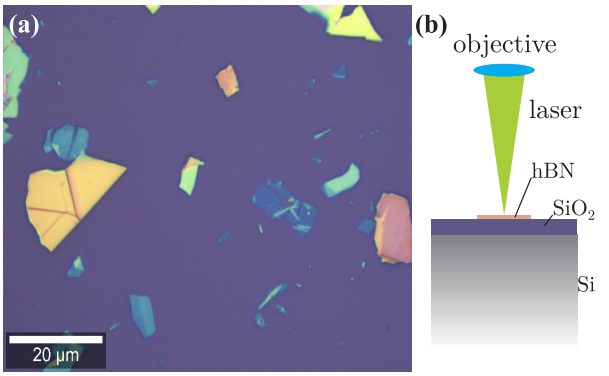

FIG. 1. Microscope image of the sample surface (a) and the schematic sample structure (b). (a) White light microscope image of exfoliated hBN flakes with varying thicknesses. With growing layer number, the flakes change color from green over yellow and orange to red and then gradually shift back to green and so on. (b) Schematic illustration of the sample structure cross section. The incoming laser light is focused on the sample surface, and the scattered light is collected with the same objective (backscattering geometry).

around 1 μm^2.[22] The optical signal was detected with a liquid-nitrogen-cooled CCD camera, attached to a 500 mm spectrometer. The exposure time (integration time) was typically 10 s with one single accumulation for a full spectrum with 0.26 nm (or 0.9 meV) resolution. The laser power was set to 500 μW. In the other setup, a commercial Raman microscope (WITec alpha300 RA), three different excitation wavelengths (457, 532, and 633 nm) could be used. All of the Raman spectra measured in this setup were done with one single accumulation and an exposure time of 20 s for all lasers. The laser power of the 457 and 532 nm laser was set to 2 mW, and the power of the 633 nm laser was 10 mW. Before all Raman measurements, the spot size was focused and minimized to assure that we had the sample surface within the focal depth of the Gaussian beam. As mentioned earlier, the thicknesses of the flakes were determined by AFM (Bruker Dimension Icon).

Shown in Fig. 2 are Raman spectra, taken on hBN flakes with different thicknesses. All spectra in this work were subtracted by the baseline and were divided by the exposure time to get the signal in counts per second (cps). The first peak at 519 cm^{-1} is the Si Raman signal.[23] Above 780 cm^{-1}, the intensity is scaled by a factor of 10 for better visibility of the weaker Raman signals (right axis). The broad peak between 930 and 1030 cm^{-1} is assigned to a Si multi-phonon scattering process (SiMP).[23] The peak at around 1365 cm^{-1} is the Raman signal of hBN.[24,25] Looking at the intensities of the different Raman signals for increasing hBN layer thickness (bottom to top), we can already observe a non-monotonic development of the peak height. From a thickness of $d_{hBN} = 19$ to $d_{hBN} = 65.5$ nm, the Si peaks drop in intensity and then increase again. At around $d_{hBN} = 120$ nm, maximum intensity is observed, and with increasing hBN layer thickness, the intensity decreases again.

For the hBN Raman peak, we observe a different behavior, as the Raman intensity does not decrease from $d_{hBN} = 120$ to $d_{hBN} = 140$ nm. This can be explained by the fact that with increasing layer thickness, the volume in which hBN Raman scattering can take place also increases, while the excitation volume remains constant for

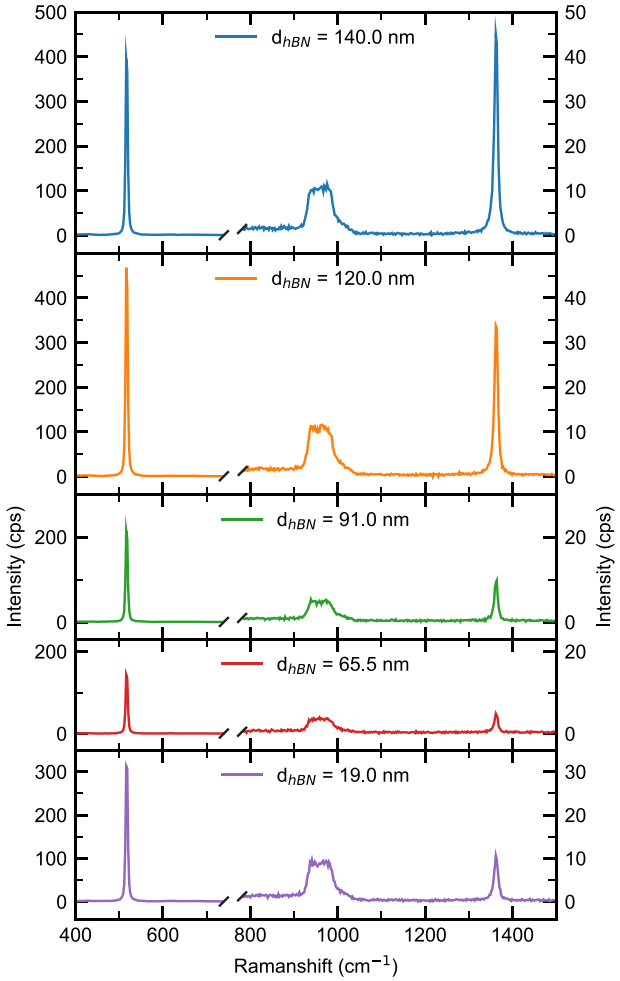

FIG. 2. Raman spectra of hBN flakes with varying thicknesses between 19 and 140 nm on a Si/SiO_2 substrate, recorded with an excitation wavelength of 532 nm. The right side of the spectra with the SiMP Raman peak between 930 and 1030 cm^{-1} and the hBN peak at 1390 cm^{-1} is plotted with an enlarged scale, to better visualize these weaker peaks. A non-linear behavior of the intensities with the hBN layer thickness is observed.

the other materials. This offsets the trend in the other Raman signals. Because the thickness of the hBN is less than the focal depth, the effective volume increases linearly with increasing hBN thickness. This agrees with the findings of Rodriguez–Martinez, who found a Lambert–Beer-like increase in the signal,[16] which can be approximated as linear for thin samples like those investigated here.

We took nine differently colored hBN flakes and determined their thickness by AFM. The thicknesses ranged from 5 to 190 nm. A monolayer of hBN has an AFM-measured thickness of around 0.4 nm, a bilayer of 0.8 nm, and a trilayer of 1.2 nm.[26,27] This corresponds to measured hBN flakes from around 12 layers up to 475 layers. By plotting the Raman peak intensity against the layer thickness of the hBN flakes, the oscillating behavior becomes more apparent. In Fig. 3, the intensity of the reflected laser light and the Si Raman signal (519 cm^{-1})[23] are plotted as a function of thickness. The relative

21 August 2023 14:13:57

© Author(s) 2023

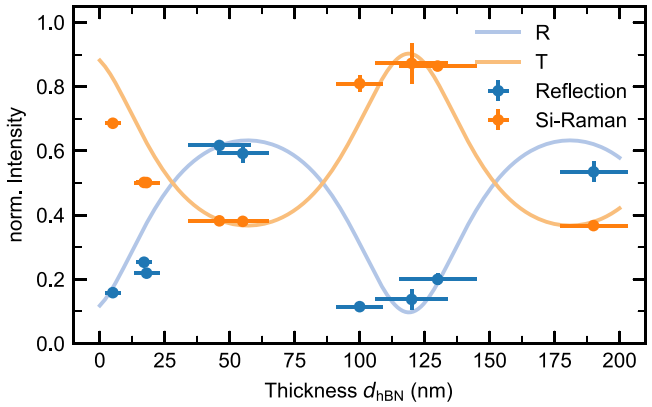

FIG. 3. Intensities of Si Raman peak (orange) and laser reflection peak (blue) are plotted against the hBN flake thickness together with the theoretical curves (solid lines) for transmissivity (orange) and reflectivity (blue) based on the TMA model. All Raman peak intensities are divided by the same fixed normalization factor.

reflection intensity was obtained by detecting the backscattered laser light, which was strongly suppressed but not completely eliminated from the spectrum. Figure 3 shows that the reflected laser light and the Raman peak exhibit opposite oscillation behavior: When the reflected laser light gains in intensity, the Raman peak gets weaker and vice versa.

To explain this behavior, we employ the transfer-matrix algorithm (TMA),[14] which is commonly used to model light propagation in a multi-layer system like our sample structure. For perpendicular incoming light (wavelength λ_0), the transfer matrix for each layer is[15]

$$M_j = \begin{pmatrix} \cos(k_0 n_j d_j) & \frac{1}{in_j}\sin(k_0 n_j d_j) \\ -in_j \sin(k_0 n_j d_j) & \cos(k_0 n_j d_j) \end{pmatrix}. \quad (1)$$

Here, n_j is the refractive index, d_j is the thickness of layer j (j = hBN, SiO_2), and $k_0 = \frac{2\pi}{\lambda_0}$. The product of all matrices gives the transfer matrix of the entire layer system,

$$M = \prod_j M_j. \quad (2)$$

From the elements m_{lk} of M, it is possible to calculate the reflection and transmission coefficients,

$$r = \frac{(m_{11} + m_{12}n_l)n_f - (m_{21} + m_{22}n_l)}{(m_{11} + m_{12}n_l)n_f + (m_{21} + m_{22}n_l)}, \quad (3a)$$

$$t = \frac{2n_f}{(m_{11} + m_{12}n_l)n_f + (m_{21} + m_{22}n_l)}, \quad (3b)$$

where n_f is the refractive index of the first material (air, $n_f = n_{air}$) and n_l is the refractive index of the last material (Si, $n_l = n_{Si}$). From r and t, we can calculate the reflectivity $R = |r|^2$ and transmissivity $T = \frac{n_l}{n_f}|t|^2 = \frac{n_{Si}}{n_{air}}|t|^2$. In the last step, the material parameters are inserted for each layer j, like the excitation wavelength λ_0, the thickness of the SiO_2 layer d_{SiO_2}, and the corresponding wavelength-dependent refractive indices $[n_{SiO_2}(\lambda_0)$[28] and $n_{hBN}(\lambda_0)]$.[29] The calculated reflectivity and transmissivity for a laser wavelength of 532 nm and the SiO_2 layer thickness of 285 nm, plotted over the hBN thickness, are also shown in Fig. 3. Apart from a slight adjustment of the SiO_2 thickness (within the error margin given by the supplier), there are no fitting parameters. The curves are calculated with the given parameters, such as the refractive indices (n_j), the vacuum wavelength of the laser (λ_0), and the given thickness of the SiO_2. The thickness of the hBN was independently determined by atomic force microscopy. Also note that, by placing the layered structure within the focal depth of the objective lens, we made sure that the wavefronts are parallel to the sample surface.[30] Therefore, the transfer matrix formula for perpendicular incoming light can be used.

For the measurements shown so far, we only used a green laser as the excitation source. To further substantiate our findings, we performed a second set of experiments with three different excitation laser wavelengths (λ_0 = 457, 532, and 633 nm). On a new sample, Raman spectra of 22 flakes with different thicknesses were recorded.

In Fig. 4, the intensities of the SiMP and the hBN Raman signal are plotted vs the hBN layer thickness for the three excitation wavelengths. The intensity of the SiMP signal is the average intensity between 930 and 1030 cm^{-1}. The solid curves are again calculated by the TMA, taking into account the refractive indices of the materials for the different excitation wavelengths.

In Fig. 4 (left), it can be seen that the oscillating behavior of the SiMP peak for 532 nm excitation is similar to the one shown in Fig. 3. In comparison with the two additional excitation wavelengths, we observe that the period of the oscillations increases with increasing hBN thickness. This is expected, as the oscillations stem from commensurability between the wavelength and the thickness of the dielectric. When we use the respective parameters in the TMA, the calculated curves exhibit the same behavior as the experimental data points for all three laser wavelengths. This shows that our model calculation is sufficient to describe the observed behavior in dependence of both the hBN thickness and the excitation wavelength. Especially, as already mentioned, there is no kind of fitting parameter involved in the theoretical curve. Only the intensity of the data points was normalized.

As mentioned earlier, for the hBN signal (shown in the right part of Fig. 4), we use a linear approximation to take into account the increasing Raman intensity with increasing number of hBN layers. This approximation, together with the TMA model, fits the oscillating data points quite well, but with a slightly larger deviation compared to the SiMP peak. In particular, the data for 633 nm show some deviation from the model, which might stem from the very simple linear approximation. We also included other approximations in our model calculation to account for the increasing scattering volume of the hBN flakes, such as a Lambert–Beer-like or a square-root behavior. However, none of these resulted in a better agreement with the data points. Similar to the SiMP signal, the hBN peaks also show an increase in the period with increasing excitation wavelength. Again, it is possible to model the changes in Raman intensity with the TMA model, using the appropriate parameters and without any fitting except a constant for the linear increase in the scattering volume for the hBN Raman peak.

Finally, we would like to briefly discuss why the Si and hBN Raman signals are enhanced up to almost 60% when the *transmission* coefficient is at maximum (rather than the reflection coefficient, see Fig. 3), even though the measurements were done in backscattering

21 August 2023 14:13:57

© Author(s) 2023

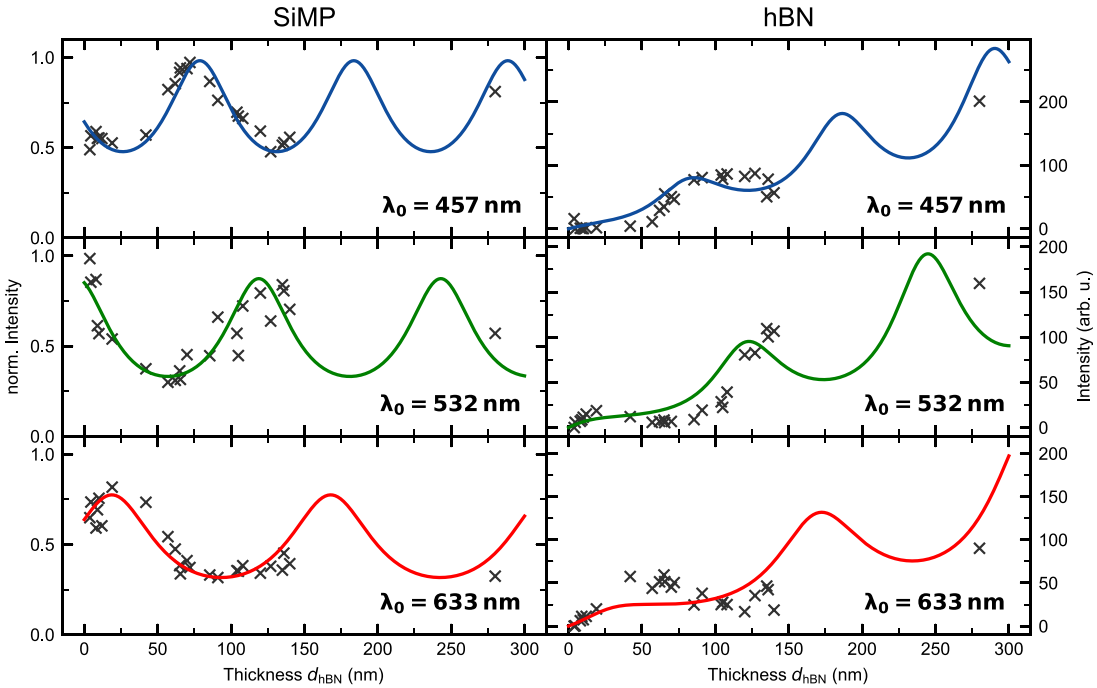

FIG. 4. Data points: Normalized Raman intensity as a function of the hBN layer thickness for the SiMP (left) and the hBN (right) Raman line, for the three different excitation lasers (457, 532, and 633 nm). The solid lines stand for the transmissivity of the TMA model for each excitation wavelength. In the case of the hBN TMA model plots, there is a linear intensity increase accounting for the increased scattering volume superimposed.

geometry. For maximum transmission, the dielectric layer (SiO_2 plus hBN in our case) serves as a resonator, where light is reflected back and forth, and the partial waves from both interfaces interfere constructively. This leads to an amplification of the light intensity within the layer. We, therefore, conclude that the improved Raman signals are caused by a more efficient coupling between the impinging laser light and the dielectric layer that contains the Raman-active media.

The interference colors that can easily be observed under an optical microscope (see Fig. 1) are, therefore, not only helpful to quickly approximate the thickness of the material under investigation.[16–20] They can also be used to select flakes with optimum thickness for any specific excitation wavelength. Alternatively, for a given flake, the optimal excitation wavelength can be chosen for the highest emission intensity. As seen in Fig. 3, the condition with the highest emission intensity comes with the additional benefit that the spurious reflected laser light will be at a minimum. This can lead to a drastically improved signal-to-noise ratio for the investigated optical process, be it Raman, bulk photoluminescence, or fluorescence from single defect emitters.

In summary, we performed Raman measurements with different excitation wavelengths for hBN flakes of various thicknesses. We observed thickness-depended oscillations of the Raman signals from the different materials in our layered system: hBN, SiO_2, and Si. It could be shown that a transfer-matrix approach can be used to well describe the oscillating behavior of both the reflected and the emitted Raman signal. To account for the thickness variation of the hBN, and therefore, a variation of the volume that is available for Raman excitation, we used a simple linear dependence, which could reproduce the experimental data well. Our findings are of general applicability for any layered material system to choose the optimum thickness for a given excitation wavelength or, vice versa, to choose the best-suited laser wavelength for a particular layer or flake. Even dissipative materials with an imaginary contribution to the refractive index can be treated using the TMA model. As long as the penetration depth is much larger than the optical thickness of the material, (damped) oscillations in the transmission and reflection coefficients are seen in the calculations.

The funding by the Deutsche Forschungsgemeinschaft (DFG, German Research Foundation) within projects SFB 1242, ID No. 278162697, IRTG 2803-461605777, and INST-429784087 is gratefully acknowledged.

AUTHOR DECLARATIONS

Conflict of Interest

The authors have no conflicts to disclose.

Author Contributions

Felix Schaumburg: Conceptualization (equal); Data curation (lead); Formal analysis (lead); Investigation (lead); Methodology (equal); Validation (equal); Visualization (lead); Writing – original draft (equal); Writing – review & editing (equal). **Stephan Sleziona:** Investigation (equal); Validation (supporting); Visualization

21 August 2023 14:13:57

© Author(s) 2023

(supporting); Writing – review & editing (equal). **Marcel Zöllner:** Conceptualization (equal); Investigation (supporting); Methodology (supporting); Supervision (supporting); Visualization (equal); Writing – review & editing (equal). **Vasilis Dergianlis:** Conceptualization (equal); Investigation (equal); Methodology (equal); Supervision (equal). **Marika Schleberger:** Funding acquisition (equal); Project administration (equal); Resources (equal); Supervision (equal); Writing – review & editing (equal). **Martin Geller:** Formal analysis (equal); Funding acquisition (equal); Methodology (equal); Project administration (equal); Resources (equal); Supervision (equal); Writing – review & editing (equal). **Axel Lorke:** Conceptualization (equal); Formal analysis (equal); Funding acquisition (lead); Methodology (equal); Project administration (lead); Supervision (lead); Validation (equal); Visualization (equal); Writing – original draft (equal); Writing – review & editing (equal). **Günther M. Prinz:** Conceptualization (equal); Formal analysis (equal); Investigation (equal); Methodology (equal); Supervision (equal); Validation (equal); Visualization (equal); Writing – original draft (equal); Writing – review & editing (equal).

DATA AVAILABILITY

The data that support the findings of this study are available from the corresponding authors upon reasonable request.

REFERENCES

[1]K. S. Novoselov, A. K. Geim, S. V. Morozov, D. Jiang, Y. Zhang, S. V. Dubonos, I. V. Grigorieva, and A. A. Firsov, Science **306**, 666 (2004).
[2]A. V. Kretinin, Y. Cao, J. S. Tu, G. L. Yu, R. Jalil, K. S. Novoselov, S. J. Haigh, A. Gholinia, A. Mishchenko, M. Lozada, T. Georgiou, C. R. Woods, F. Withers, P. Blake, G. Eda, A. Wirsig, C. Hucho, K. Watanabe, T. Taniguchi, A. K. Geim, and R. V. Gorbachev, Nano Lett. **14**, 3270 (2014).
[3]J. Yu, X. Kuang, J. Zhong, L. Cao, C. Zeng, J. Ding, C. Cong, S. Wang, P. Dai, X. Yue, Z. Liu, and Y. Liu, Opt. Express **28**, 13260 (2020).
[4]A. Micevic, N. Pettinger, A. Hötger, L. Sigl, M. Florian, T. Taniguchi, K. Watanabe, K. Müller, J. J. Finley, C. Kastl, and A. W. Holleitner, Appl. Phys. Lett. **121**, 183101 (2022).
[5]H. L. Stern, Q. Gu, J. Jarman, S. Eizagirre Barker, N. Mendelson, D. Chugh, S. Schott, H. H. Tan, H. Sirringhaus, I. Aharonovich, and M. Atatüre, Nat. Commun. **13**(1), 618 (2022).
[6]S. White, C. Stewart, A. S. Solntsev, C. Li, M. Toth, M. Kianinia, and I. Aharonovich, Optica **8**, 1153 (2021).
[7]M. Kianinia, C. Bradac, B. Sontheimer, F. Wang, T. T. Tran, M. Nguyen, S. Kim, Z.-Q. Xu, D. Jin, A. W. Schell, C. J. Lobo, I. Aharonovich, and M. Toth, Nat. Commun. **9**, 874 (2018).
[8]G. Grosso, H. Moon, B. Lienhard, S. Ali, D. K. Efetov, M. M. Furchi, P. Jarillo-Herrero, M. J. Ford, I. Aharonovich, and D. Englund, Nat. Commun. **8**, 705 (2017).
[9]Z. Q. Xu, C. Elbadawi, T. T. Tran, M. Kianinia, X. Li, D. Liu, T. B. Hoffman, M. Nguyen, S. Kim, J. H. Edgar, X. Wu, L. Song, S. Ali, M. Ford, M. Toth, and I. Aharonovich, Nanoscale **10**, 7957 (2018).
[10]F. Hayee, L. Yu, J. L. Zhang, C. J. Ciccarino, M. Nguyen, A. F. Marshall, I. Aharonovich, J. Vučković, P. Narang, T. F. Heinz, and J. A. Dionne, Nat. Mater. **19**, 534 (2020).
[11]H. Akbari, S. Biswas, P. K. Jha, J. Wong, B. Vest, and H. A. Atwater, Nano Lett. **22**, 7798 (2022).
[12]J. Ziegler, R. Klaiss, A. Blaikie, D. Miller, V. R. Horowitz, and B. J. Alemán, Nano Lett. **19**, 2121 (2019).
[13]N. J. Guo, W. Liu, Z. P. Li, Y. Z. Yang, S. Yu, Y. Meng, Z. A. Wang, X. D. Zeng, F. F. Yan, Q. Li, J. F. Wang, J. S. Xu, Y. T. Wang, J. S. Tang, C. F. Li, and G. C. Guo, ACS Omega **7**, 1733 (2022).
[14]L. R. Ram-Mohan, K. H. Yoo, and R. L. Aggarwal, Phys. Rev. B **38**, 6151 (1988).
[15]M. Born and E. Wolf, *Principles of Optics*, 7th (expanded) anniversary edition and 60th anniversary edition (Cambridge University Press, Cambridge, UK, 1999).
[16]X. Rodríguez-Martínez, M. S. Vezie, X. Shi, I. McCulloch, J. Nelson, A. R. Goñi, and M. Campoy-Quiles, J. Mater. Chem. **5**, 7270 (2017).
[17]S. Akcöltekin, M. El Kharrazi, B. Köhler, A. Lorke, and M. Schleberger, Nanotechnology **20**, 155601 (2009).
[18]P. Blake, E. W. Hill, A. H. Castro Neto, K. S. Novoselov, D. Jiang, R. Yang, T. J. Booth, and A. K. Geim, Appl. Phys. Lett. **91**, 063124 (2007).
[19]Z. H. Ni, H. M. Wang, J. Kasim, H. M. Fan, T. Yu, Y. H. Wu, Y. P. Feng, and Z. X. Shen, Nano Lett. **7**, 2758 (2007).
[20]C. Hsu, R. Frisenda, R. Schmidt, A. Arora, S. M. de Vasconcellos, R. Bratschitsch, H. S. J. van der Zant, and A. Castellanos-Gomez, Adv. Opt. Mater. **7**, 1900239 (2019).
[21]R. T. Holm, S. W. McKnight, E. D. Palik, and W. Lukosz, Appl. Opt. **21**, 2512 (1982).
[22]A. Asaithambi, R. Kozubek, G. M. Prinz, F. Reale, E. Pollmann, M. Ney, C. Mattevi, M. Schleberger, and A. Lorke, Phys. Status Solidi RRL **15**, 2000466 (2021).
[23]P. A. Temple and C. E. Hathaway, Phys. Rev. B **7**, 3685 (1973).
[24]L. H. Li and Y. Chen, Adv. Funct. Mater. **26**, 2594 (2016).
[25]N. Basu, M. S. Satya Bharathi, M. Sharma, K. Yadav, A. S. Parmar, V. R. Soma, and J. Lahiri, J. Nanomater. **11**, 622 (2021).
[26]R. V. Gorbachev, I. Riaz, R. R. Nair, R. Jalil, L. Britnell, B. D. Belle, E. W. Hill, K. S. Novoselov, K. Watanabe, T. Taniguchi, A. K. Geim, and P. Blake, Small **7**, 465 (2011).
[27]L. H. Li, J. Cervenka, K. Watanabe, T. Taniguchi, and Y. Chen, ACS Nano **8**, 1457 (2014).
[28]I. H. Malitson, J. Opt. Soc. Am. **55**, 1205 (1965).
[29]S.-Y. Lee, T.-Y. Jeong, S. Jung, and K.-J. Yee, Phys. Status Solidi B **256**, 1800417 (2019).
[30]H. J. Eichler, J. Eichler, and O. Lux, "Laser beam propagation in free space," in *Lasers: Basics, Advances and Applications* (Springer International Publishing, Cham, 2018), pp. 207–229.

21 August 2023 14:13:57

© Author(s) 2023